

Article

Proposed Model For Shale Compaction Kinetics: Forward Depositional Model

James Edward Smith ^{1,*} and Edward Millard Smith-Rowland ²

¹ Phillips Petroleum Company retired, 1209 Harris Dr, Bartlesville, OK 74006, USA

² Alion Science and Technology, 3113 Edgewood Rd, Ellicott City, MD 21043-3419, USA; esmithrowland@gmail.com

* Correspondence: edsmith6@hotmail.com

Received: date; Accepted: date; Published: date



Abstract: Wind, rain and snow combine to disintegrate, dissolve or react with land and vegetation, and to move altered solids lower as required by gravitational forces. The finest solids are deposited in low, less turbulent areas, such as lake bottoms and sea floors. They sometimes stack up to thicknesses of kilometers, and begin compacting. These sediment sections are called shales, and as initially deposited in water, shales can have porosities up to 50-80% water. As they are buried, many alteration products from oil to slate are produced due to overburden and temperature increases, making them important to study. Besides initial mechanical compaction, other mechanisms can contribute to reduction of porosity. A preceding paper showed that an important process is pressure solution of some part of the shale minerals. Without naming the mineral(s) involved, it postulated that the greater product of the water and pore interfaces, the faster the reaction would proceed. This term is $\varphi^{4m/3}(1 - \varphi)^{4n/3}$, where m and n are close to unity, and the large exponents, $3/4$, recognize that the reaction occurs at the molecular scale at which the surfaces are rough. A second term, $\exp(-E/RT)$, indicates that the reaction is impeded by a quantum energy barrier, E , with diminished impeding power as increased available thermal energy, represented by the absolute temperature, T , becomes available at greater depths in the Earth. These two factors combine to allow porosity φ to reduce with time, or equivalently for the fraction of solids, $(1 - \varphi)$, to increase with time,

$$\left. \frac{\partial(\ln(1-\varphi))}{\partial t} \right|_{\sigma} = (\varphi)^{4m/3}(1 - \varphi)^{4n/3} A e^{-E/(RT)}.$$

It is recognized here that this equation provides snapshots, at all times during the burial, of the sediments at each depth. This visualization is more appropriate than the continuous time representation with a derivative, as the actual reaction is quantized.

A known time-depth history for a shale section would allow determination of the parameters m, n, A , and E . Lacking this known history, a constant rate of solids deposition, r , can be assumed and these parameters can then be determined. This was done for six shale sections, and for a wide range of deposition rates. Satisfactory results were obtained over this range of r 's using the previously determined m and n , and porosity and temperature profiles, only varying A and E . The derived activation energy E is close to that for pressure solution of SiO_2 , which may comprise 20-50% of shales.

Keywords: depositional model; forward model; shale compaction; kinetics; activation energy; pore interfaces; grain interfaces; fractals

1. Introduction

A kinetic equation previously presented [1] allowed one to determine the time history of porosity of a given shale section in terms of four constant parameters, m, n, A and activation energy E :

$$\left. \frac{\partial(\ln(1 - \varphi))}{\partial t} \right|_{\sigma} = (\varphi)^{4m/3} (1 - \varphi)^{4n/3} A e^{-E/(RT)}. \quad (1)$$

The right hand side is analogous to customary chemical kinetic equations, and anticipates that compaction occurs because some shale component either dissolves into pore water, or moves along the mineral-water interface, and then precipitates to infill pore space. Constant 'A' has units /time, but cannot be interpreted or separately computed as a collision frequency, as is done in purely fluid systems. It involves ensembles of changing grain-to-grain contact areas, morphologies, geometrical restrictions and complications among inhomogeneous solids, many of which may not participate.

The first two dimensionless parameters, m and n, were estimated by first noting that the time derivative on the left would be zero at zero porosity, so that the first non-vanishing term in a Taylor series representation would be proportional to φ . For a particular actual shale porosity profile, m and n can be varied to make $\varphi * [(\varphi)^{-4m/3} (1 - \varphi)^{-4n/3}]$ close to constant over the deeper part, as was illustrated for six sections. The exponents are not near 2/3, as expected for mathematically flat interfaces, but reflect the rough interfaces at the molecular level. The 'deeper part' restriction arises because the compaction mechanism is pressure solution, and this necessarily disappears at the surface where there is no overburden. Other mechanisms like mechanical compaction and bioturbation contribute more at shallow depths. The six example shales used here are the same as in [1] and the same m, n and temperature profiles are used. The included temperatures are extended to 25 deg C [2] instead of the less inclusive 30-40 deg C as previously. This changes A and E slightly. The A values reported here for the largest deposition rate replace those in [1] Tables 2 and 3 of which were incorrectly reported. 'Deeper part', as before excludes porosities bigger than 0.5 if measured or reported.

The model parameters to be derived here show some variation. Current understanding and information is not complete enough to choose among causes. For instance, there are six varieties of quartz for which different solubilities have been measured at 25 dec C, and one cannot be certain whether derived pressure solution parameters will also vary for this one mineral. Mineral activation energies E vary with pH [3]. Other mineral cements such as CaCO₃ are potential candidates [3]. Variations could be a consequence of the model, a shale property, or experimental uncertainty. Deposition rates, discussed here, are another source of variation, as are temperature variations over geologic time or vertically.

Probably the source of pressure solution/compaction is an abundant mineral fraction. SiO₂ qualifies, as it is usually 20-50% of shales, the other largest fraction being clay minerals which also contain SiO₄⁻⁴ as framework. Reactions such as montmorillonite to illite can sometimes be a source of SiO₂. Additionally, quartz is the last major mineral to freeze out of mafic materials, and thus is briefly a pore fluid and coats minerals which solidified earlier in the Bowen's reaction series.

As a footnote, a compendium of shale porosities [4] shows only greater than zero porosities for shales or slates.

If the actual deposition history of a shale section were known, it could be put into the left hand side (LHS) of equation 1 and the right hand side (RHS) parameters A and E could be determined. As mentioned, m and n will be unchanged here.

2. Development

As the deposition histories are not known, the missing link between deposition time and depth is required to continue. We assume a constant rate of solids deposition, r , in mm/y or km/Ma, for the entire section and thus obtain A and E. This is done successfully for a large range, 0.2 to 20 km/Ma, for each of the six example shales, which insures that actual complicated depositional histories can be covered.

The lower geologic time boundary, t_{g0} , and upper geologic time boundary, t_{g1} , are known. t_0 is the top of the shale section and t_b the bottom. Time is reckoned positive backward from the present. The shale deposition time interval is placed in the middle of the geologic time interval:

$$t_{z=0} = t_{g0} + \Delta \quad (2)$$

$$t_{z=b} = t_{g1} - \Delta \quad (3)$$

Δ is large when the solids deposition rate is large and will shrink to zero as the deposition rate r declines. The assumption of constant r allows Δ to be computed. As stated, constant r within a section links time and depth, z :

$$dt = (1/r)(1 - \varphi(z))dz \quad (4)$$

$$t_{z=b} - t_{z=0} = (1/r) \int_{z=0}^{z=b} (1 - \varphi_z) dz \quad (5)$$

and

$$t_{z=b} - t_{z=0} = (t_{g1} - t_{g0}) - 2 * \Delta. \quad (6)$$

Equating the right hand sides RHS gives

$$\Delta = 1/2 * [(t_{g1} - t_{g0}) - [t_{z=b} - t_{z=0}]]. \quad (7)$$

The integral (5) can be numerically evaluated by dividing $t_{z=0}$ through $t_{z=b}$ into many, N , equal small intervals $\Delta = z_i - z_{i-1}$,

$$t_{z=b} - t_{z=0} = (\Delta/r) \sum_{i=1}^{i=N} (1 - \varphi(z_i)), \quad (8)$$

where $t_{z=0}$ and $t_{z=b}$ are given by (2) and (3). In general at any depth z_i within the section,

$$t_{z=z_i} = t_{z=z_0} + (\Delta/r) \sum_{z_j=1}^{z_j=i} [1 - \varphi(z_j)] \quad (9)$$

With the equation (9) estimate of the time since deposition, equation (1) becomes, for each $i = 1$ through N ,

$$[\ln(1 - \varphi_i) - \ln(1 - \varphi_0)]/t_i = \varphi_i^{4m/3} (1 - \varphi_i)^{4n/3} A \exp[-E/(RT_i)] \quad (10)$$

The abbreviation $t_{z=z_i} = t_i$ is used here.

This is the desired result, allowing parameters A and E to be obtained from the depositional history of the shale section on the LHS.

3. Results

For these calculations, for this mechanism, the porosity extrapolated to $z = 0$ is estimated for simplicity as 0.5 for all wells/sections [5–9]. Reported actual surface porosities are sometimes more or less, or were omitted.


Moving all porosity terms to the left of equation (10) and taking the logarithm of each side yields a linear equation with intercept $\ln(A)$ and slope E . Table 1 gives the derived E and A for a broad range of realistic deposition rates, r , for each section or well studied.

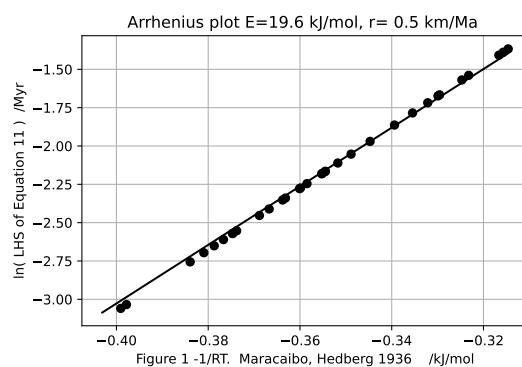
As contrasting examples, this plot is given for the Maracaibo well[9], Figure 1, and the Macran1 section [6], Figure 2. A low solids deposition rate of 0.5 km per million years is used. Figures for all six sections were previously given [1] for very high, >20 km/Ma, deposition rates such that Δ is maximum.

The Maracaibo porosities were measured on hand samples. Porosities were fitted with a straight line which omitted large near-surface porosities and made deeper porosities seem to go to zero too quickly. Experimental porosities about 36% left out. The well was drilled in or near a shallow lake in a tropical climate. The Macran-1 data were derived from seismic data with the maximum porosity reported as 69%. The environment was deep cold ocean.

This completes the forward model of deposition and compaction of these six shales. The procedure is expected to work for most shale sections, if not strongly disturbed.

Table 1. Section deposition rates and parameter fits.

Example,  Properties	r km/Ma	E kJ/mol	A /s * 10 ⁻¹²	φ std dev	φ avg dev	$\varphi - \varphi_{calc}$ max dif
Akita	0.2	30.8	43	0.05	0.00	0.05
5-149 Ma	0.3	31.1	49	0.04	0.00	0.04
m,n = 0.95,1.	1	31.6	59	0.04	0.00	0.04
t >= 25°C	4	31.8	62	0.04	0.00	0.04
$\varphi_0=0.5$	20	31.8	64	0.04	0.00	-0.04
Makran1	0.2	17.2	1.4	0.01	0.0	0.03
2.6 - 66 Ma	0.3	18.1	2.1	0.01	0.00	0.03
m,n = 0.85,1.0	1	19.7	4.0	0.01	0.00	0.03
t >= 25°C	4	20.3	5.1	0.01	0.00	0.02
$\varphi_0=0.5$	20	20.4	5.4	0.00	0.00	0.03
Makran2	0.2	14.4	0.9	0.06	0.00	-0.18
2.6 - 66 Ma	0.3	15.4	1.3	0.06	0.00	-0.18
m,n = 0.85,0.95	1	17.8	2.5	0.06	0.00	-0.17
t >= 25°C	4	17.5	3.2	0.06	0.00	-0.17
$\varphi_0=0.5$	20	17.7	3.4	0.06	0.00	-0.17
"SuluSea"	0.2	12.3	0.55	0.01	0.00	0.01
0 - 23 Ma	0.3	13.9	1.1	0.01	0.00	0.04
m,n = 0.9,0.8	1	17.4	4.6	0.01	0.00	0.04
t >= 25°C	4	19.0	8.9	0.01	0.00	0.04
$\varphi_0=0.5$	20	19.5	11.	0.01	0.00	0.04
Oklahoma	0.2	31.4	44	0.04	0.02	-0.07
254-323 Ma	0.3	31.5	46	0.04	0.02	-0.08
m,n = 0.85,1.0	1	31.6	48	0.04	0.00	-0.09
t >= 25°C	4	31.6	49	0.05	0.02	-0.08
$\varphi_0=0.5$	20	31.6	49	0.05	0.02	-0.08
Maracaibo	0.2	18.4	2.4	0.03	0.00	-0.10
2.6-66 Ma	0.3	19.1	3.1	0.03	0.00	-0.10
m,n = 0.9,0.9	1.0	20.0	4.5	0.03	0.00	-0.10
t >= 25°C	4		5.2	0.03	0.00	-0.10
$\varphi_0=0.5$	20	20.4	20.4	0.03	0.00	-0.10

**Figure 1.** Maracaibo well samples.

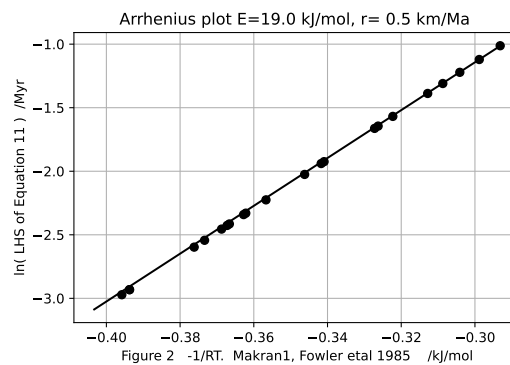


Figure 2. Macran1 seismic section.

A check can be made to see how well the derived parameters m, n, A and E reproduce the known shale porosity profiles. Equation (10) rearranges to

$$\varphi_i = 1 - (1 - \varphi_0) \exp[t_i \varphi(i)^{4m/3} (1 - \varphi(i))^{4n/3} A \exp[-E/(RT_i)]] \quad (11)$$

with all four fixed parameters on the right to estimate φ on the left. Table 1 gives the mean and standard deviations of the errors, and the error of maximum magnitude at the tops or bottoms of the sections. This maximum error is small for three of the wells but large and negative for the Macron 2, the Oklahoma, and the Maracaibo sections. The Macron 2 section, in the Macron accretionary prism, has porosities 30–40% less than the Macron 1 in the nearby abyssal plain at similar sediment depths[6]. This reduced porosity is thought due to greater horizontal stress. This same horizontal stress effect is in the Oklahoma well [8,9]. The Maracaibo location was thought to be free of excess horizontal stress[9]. Fresher, perhaps relatively acidic water in this lake, which is fed by tropical rivers, suggests one approach to explaining a lower porosity.

These discrepancies suggest a 3-dimensional compaction model is needed, but are useful in detecting horizontal forces.

4. Discussion

Several categories of unanswered questions come up in this model, and are listed as potential experimental problems, but not answered here.

- 1- Is more than one type of mineral pressure solution occurring among different wells or in each well?
- 4- Variations of stress, both positive and negative, lead to increased solubility of shale minerals[2]. Are local vertical and horizontal stresses the only drivers? What contributions do quakes and crustal movements make? What is the minimum time that a change in stress can occur and produce pressure solution?
5. How small can effective stresses be, and how small can a time increment be to produce pressure solution results?
2. Will rapid porosity reduction by pressure solution outrun pore water reduction in very low permeability environments, resulting in lowered grain-to-grain stress? How does this balance out?
3. The successful forward modeling here of a wide range of deposition rates for each shale section indicates that burial time for shales is of secondary importance. Temperature, stress, and stress variations seem more important.

These questions highlight that tidal forces were part of the proposed pressure solution mechanism

used here and were initially ignored. The vertical force per unit area of supporting grains, Λ , is given by the ratio of the vertical force per unit area, σ , divided by the area of the supporting grains, $(1 - \varphi)$:

$$\Lambda \equiv (S - p)/(1 - \varphi) = \sigma/(1 - \varphi). \quad (12)$$

Here the vertical force, σ , is the difference between the overburden, S , and the pore fluid pressure, p . Tidal forces are included in σ and should be separated as the time derivative is not zero, contrary to what may be imagined for σ :

$$\sigma = [\sigma * g_E/g](g/g_E) \quad (13)$$

or

$$\sigma = [\bar{\sigma}](g/g_E) \quad (14)$$

Here $\bar{\sigma}$ is the vertical stress toward the center of the earth, without Moon and Earth tidal pulls, and g/g_E is the scalar vertical part of these tidal forces which vary continuously. The latter should realistically be replaced by the vector pulls of Moon and Sun on every part of a section, these vectors rotating 360 degrees every lunar or solar day. Taking the time partial derivative with this in mind gives

$$\left. \frac{\partial(\ln \Lambda)}{\partial t} \right|_{\bar{\sigma}} = - \left. \frac{\partial(\ln(1 - \varphi))}{\partial t} \right|_{\bar{\sigma}} + "d(g/g_E)/dt" \quad (15)$$

The quote marks indicate this term stands in for the three-dimensional vector derivative. If the shales are primarily elastic over small macro-sized distances but have imperfections at sites where a few molecular diameters of extension collect, these sites might be a place to consider for pressure solution. Of note, the 'equator' of the Moon - Earth orbit can have a large vertical force component near the Moon-Earth axis, but as seen from the Moon, horizontal stretching forces toward the Earth's edges predominate, especially toward the 'poles'. This difference might be experimentally observable. Mutatis mutandis for the Sun. Additionally, the Moon was substantially closer to the Earth several hundred million years ago, and the stretching forces vary inversely as the cube of the distance.

5. References

References

1. Smith, J.E.; Smith-Rowland, E.M. Proposed method for shale compaction kinetics. *Geosciences* **2021**, *11*, 137. <https://doi.org/10.3390/geosciences11030137>
2. Miyakawa, K.; Kawabe, I. Pressure solution of quartz aggregates under low effective stress (0.42–0.61 MPa) at 25–45 deg C.
3. Palandri, J.L.; Kharaka, Y.K. A compilation of rate parameters of water-mineral interaction kinetics for application to geochemical modeling. U. S. Geological Survey Open File Report 2004-1068.
4. Manger, G.E. Porosity and bulk density of sedimentary rocks. Contributions to geochemistry. U. S. Geological Survey Bulletin 1144-E, 1963.
5. Aoyagi, K.; Asakawa, T. Primary migration theory of petroleum and its application to petroleum exploration. *Org. Geochem.* **1980**, *2*, 33–43.
6. Fowler, S.R.; White, R.S.; Loudon, K.E. Sediment dewatering in the Makran accretionary prism. *Earth Planet. Sci. Lett.* **1985**, *75*, 427–438.
7. Velde, B. Compaction trends of clay-rich deep sea sediments. *Mar. Geol.* **1996**, *133*, 193–201.
8. Athy, L.F. Density, porosity, and compaction of sedimentary rocks. *Am. Assoc. Pet. Geol. Bull.* **1930**, *14*, 1–24.
9. Hedberg, H.D. Gravitational compaction of clays and shales. *Am. J. Sci.* **1936**, *31*, 241–287.

Publisher's Note: MDPI stays neutral with regard to jurisdictional claims in published maps and institutional affiliations.



© 2020 by the authors. Licensee MDPI, Basel, Switzerland. This article is an open access article distributed under the terms and conditions of the Creative Commons Attribution (CC BY) license (<http://creativecommons.org/licenses/by/4.0/>).